J Biol Inorg Chem (2016) 21:777–792
DOI 10.1007/s00775-016-1370-y

ORIGINAL PAPER

Tyrosinase and catechol oxidase activity of copper(I) complexes supported by imidazole-based ligands: structure–reactivity correlations

Franziska Wendt[1] · Christian Näther[1] · Felix Tuczek[1]

Received: 25 February 2016 / Accepted: 8 June 2016 / Published online: 22 June 2016

Abstract Four new imidazole-based ligands, 4-((1*H*-imidazol-4-yl)methyl)-2-phenyl-4,5-dihydrooxyzole (**L_{OL}1**), 4-((1*H*-imidazol-4-yl)methyl)-2-(*tert*-butyl)-4,5-dihydrooxyzole (**L_{OL}2**), 4-((1*H*-imidazol-4-yl)methyl)-2-methyl-4,5-dihydrooxyzole (**L_{OL}3**), and *N*-(2,2-dimethylpropylidene)-2-(1-trityl-1*H*-imidazol-4-yl-)ethyl amine (**L_{imz}1**), have been synthesized. The corresponding copper(I) complexes [Cu(I)(**L_{OL}1**)(CH_3CN)]PF_6 (Cu**L_{OL}1**), [Cu(I)(**L_{OL}2**)(CH_3CN)]PF_6 (Cu**L_{OL}2**), [Cu(I)(**L_{OL}3**)(CH_3CN)]PF_6 (Cu**L_{OL}3**), [Cu(I)(**L_{imz}1**)(CH_3CN)$_2$]PF_6 (Cu**L_{imz}1**) as well as the Cu(I) complex derived from the known ligand bis(1-methylimidazol-2-yl)methane (**BIMZ**), [Cu(I)(**BIMZ**)(CH_3CN)]PF_6 (Cu**BIMZ**), are screened as catalysts for the oxidation of 3,5-di-*tert*-butylcatechol (3,5-DTBC-H_2) to 3,5-di-*tert*-butylquinone (3,5-DTBQ). The primary reaction product of these oxidations is 3,5-di-*tert*-butylsemiquinone (3,5-DTBSQ) which slowly converts to 3,5-DTBQ. Saturation kinetic studies reveal a trend of catalytic activity in the order Cu**L_{OL}3** ≈ Cu**L_{OL}1** > Cu**BIMZ** > Cu**L_{OL}2** > Cu**L_{imz}1**. Additionally, the catalytic activity of the copper(I) complexes towards the oxygenation of monophenols is investigated. As substrates 2,4-di-*tert*-butylphenol (2,4-DTBP-H), 3-*tert*-butylphenol (3-TBP-H), 4-methoxyphenol (4-MeOP-H), *N*-acetyl-L-tyrosine ethyl ester monohydrate (NATEE) and 8-hydroxyquinoline are employed. The oxygenation products are identified and characterized with the help of UV/Vis and NMR spectroscopy, mass spectrometry, and fluorescence measurements. Whereas the copper complexes with ligands containing combinations of imidazole and imine functions or two imidazole units (Cu**L_{imz}1** and Cu**BIMZ**) are found to exhibit catalytic tyrosinase activity, the systems with ligands containing oxazoline just mediate a stoichiometric conversion. Correlations between the structures of the complexes and their reactivities are discussed.

Keywords Type 3 copper enzymes · Tyrosinase · Catechol oxidase · Kinetics · Dioxygen activation

Introduction

The type 3 copper protein tyrosinase (Ty) catalyzes the *ortho*-hydroxylation of L-tyrosine to L-DOPA and the subsequent two-electron oxidation to L-DOPAquinone (monophenolase activity, Fig. 1). The active site of these proteins contains two copper centers coordinated by six histidines and binds dioxygen in a side-on bridging μ-η^2:η^2 geometry [1–3]. The oxygenation of tyrosine to L-DOPAquinone is the first step of melanin synthesis [4]. As melanin is ubiquitous, animals, plants, fungi and bacteria make use of tyrosinase [5]. The pigmentation of skin, the browning of fruits and the sclerotization of insect cuticles are all based on melanogenesis [6, 7].

The related enzyme catechol oxidase (CO) catalyzes the two-electron oxidation of catechols to *ortho*-quinones (diphenolase activity). Whereas Ty also exhibits diphenolase activity CO cannot mediate the *ortho*-hydroxylation

Dedicated to Prof. Dr. Edward I. Solomon in honor of the ACS Alfred Bader Award.

Electronic supplementary material The online version of this article (doi:10.1007/s00775-016-1370-y) contains supplementary material, which is available to authorized users.

✉ Felix Tuczek
ftuczek@ac.uni-kiel.de

[1] Institute of Inorganic Chemistry, Christian-Albrechts-University, Max-Eyth-Straße 2, 24118 Kiel, Germany

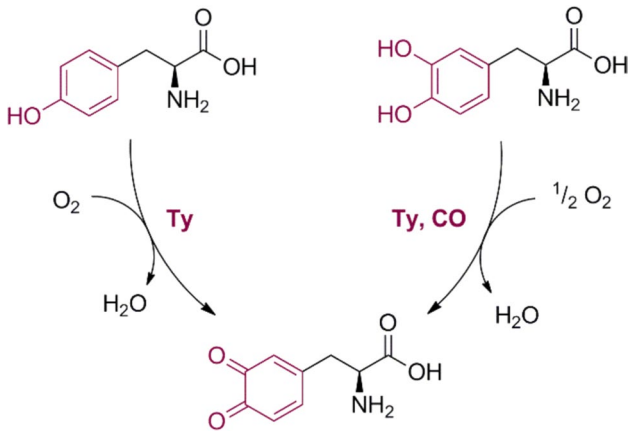

Fig. 1 Catalytic activities of tyrosinase and catechol oxidase

step involved in monophenolase activity (Fig. 1). Ty and CO are commonly referred to as phenoloxidases [8]. Recently, we discovered that the main structural difference between Ty and CO is the lack of an asparagine (Asn) in the latter enzyme. Along with a glutamate, the Asn residue activates conserved water towards deprotonation of monophenols. If Asn is missing, only diphenolase activity is observed [9].

The reproduction of tyrosinase activity by inorganic model systems catalytically oxidizing or oxygenating external phenolic substrates has a long history. In 1990, Réglier et al. presented a catalytic tyrosinase model system containing the ligand bis-2,2′-[2-(pyrid-2-yl)ethyl]-iminobiphenyl (BiPh-(impy)$_2$) (Fig. 2) [10].

In 1991, Casella and coworkers developed another model system based on the ligand α, α′-bis{bis[2-(1-methylbenzimidazol-2-yl)ethyl]-amino}-*m*-xylene (L66) [11]. The role of the Cu_2O_2 complex as the hydroxylating species in the monophenolase reaction was demonstrated in 2003 [12]. Monooxygenation of external substrates was also studied in many other systems [13–16]. Detailed mechanistic insight into the monooxygenation of external substrates was achieved by the Cu(I)DBED system (DBED = 1,2-bis(di-*tert*-butyl)ethylene-diamine) [17]. Upon exposure to dioxygen the formation of a (μ-η^2:η^2)-peroxo-dicopper(II) species was observed. Subsequent addition of a phenolate led to a bis-μ-oxo intermediate, providing the first evidence for a "ternary intermediate" (Cu + O_2 + substrate) in the course of the tyrosinase-like hydroxylation reaction. Further reaction led to a catecholato intermediate and the final product, a semiquinone complex [17, 18].

The first catalytic model system of tyrosinase based on a mononucleating ligand, [2-(pyrid-2-yl)ethyl]imino-*tert*-butane (**L$_{py}$1**) was reported by our group [19]. In 2013, Herres-Pawlis et al. presented catalytic copper(I) model

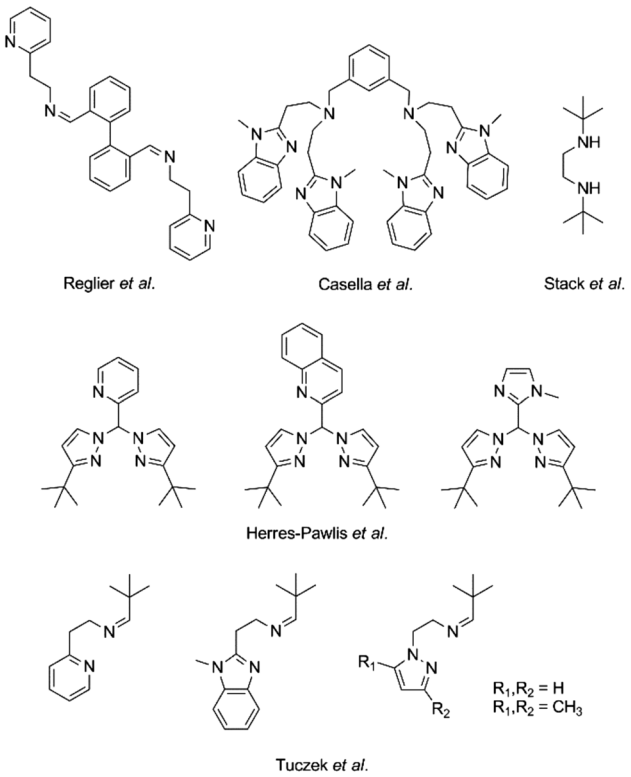

Fig. 2 Ligand designs used for tyrosinase reaction

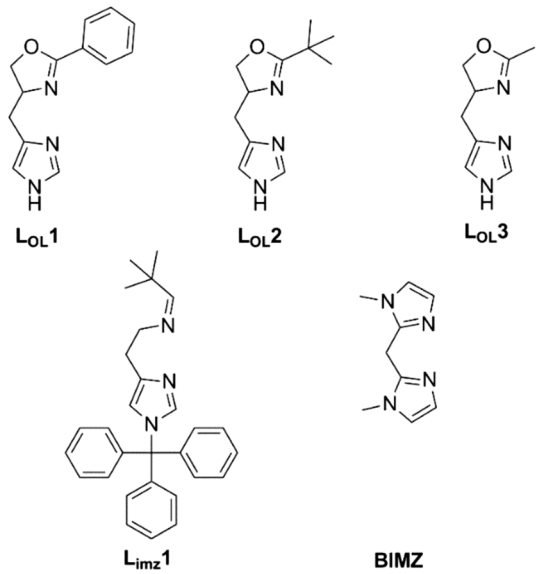

Fig. 3 Structure of bidentate imidazole-based ligands for catalytic reactions: **L$_{OL}$1-3**, **L$_{imz}$3** and **BIMZ**

systems supported by bis(pyrazolyl)methane ligands which exhibit room temperature stable peroxo intermediates [20]. More recently, Lumb et al. demonstrated catalytic conversions of different monophenols to a variety of organic products [21–26].

During the last years our group published a number of new copper(I) complexes functioning as model systems for tyrosinase [2, 19, 27–34]. Starting from the parent mononuclear complex with the ligand $\mathbf{L_{py}1}$ containing a pyridyl moiety and an imine unit, we first replaced the *N*-heterocycle by benzimidazole and pyrazole to investigate the influence of the electronic structure of the ligand on the turnover number (TON) of the corresponding copper catalyst. To expand the scope of the oxygenation reactions mediated by these systems, symmetric ligands such as di(pyrid-2-yl)methane and different bispyrazolylmethane ligands such as (1,1′-methylenebis-1*H*-pyrazole (**BPM**), 1,1′-methylenebis(3-methyl-1*H*-pyrazole) (**mBPM**), and 1,1′-methylenebis(3,5-dimethyl-1*H*-pyrazole) (**dmBPM**) were developed. The copper(I) complex of di(pyrid-2-yl) methane revealed no tyrosinase activity, in contrast to the copper(I) complexes of Cu(I)**BPM**, Cu(I)**mBPM** and Cu(I)**dmBPM**.

In this paper, we present new ligands containing imidazole moieties to model the histidine residues in the native protein (Fig. 3).

The ligand *N*-(2,2-dimethylpropylidene)-2-(1-trityl-1*H*-imidazol-4-yl-)ethyl amine ($\mathbf{L_{imz}1}$) contains an imidazole unit instead of the pyridine moiety of the parent $\mathbf{L_{py}1}$ system. The incorporated trityl residue increases the solubility in dichloromethane. Reaction with tetrakis(acetonitrile) copper(I) hexafluorophosphate leads to the copper(I) complex $[Cu(I)(\mathbf{L_{imz}1})(CH_3CN)_2]PF_6$ ($Cu\mathbf{L_{imz}1}$). Additionally, we prepared the complex $[Cu(I)(\mathbf{BIMZ})(CH_3CN)PF_6$ (Cu**BIMZ)** which is supported by the ligand bis(1-methylimidazol-2-yl)methane (**BIMZ**) containing two imidazole groups [35].

Importantly, the imine function being present in the parent ligand $\mathbf{L_{py}1}$ as well as its analogs, including $\mathbf{L_{imz}1}$, is very unstable against hydrolysis. This could be one reason for the limited TON of the resulting copper catalysts. To prevent the hydrolysis of the imine group, we replace the labile imine function of the $\mathbf{L_{imz}1}$ ligand by different oxazoline units. To gain insight into steric effects, we investigate three ligands containing different substituents adjacent to the oxazoline moiety; i.e., a phenyl group (4-((1*H*-imidazol-4-yl)methyl)-2-phenyl-4,5-dihydrooxyzole, $\mathbf{L_{OL}1}$), a *tert*-butyl group (4-((1*H*-imidazol-4-yl)methyl)-2-(*tert*-butyl)-4,5-dihydrooxyzole, $\mathbf{L_{OL}2}$), and a methyl group (4-((1*H*-imidazol-4-yl)methyl)-2-methyl-4,5-dihydrooxyzole, $\mathbf{L_{OL}3}$).

First, the catechol oxidase activity with respect to the substrate to 3,5-di-*tert*-butylcatechol (3,5-DTBC-H_2) is studied for all five copper(I) complexes ($Cu\mathbf{L_{OL}1\text{-}3}$, $Cu\mathbf{L_{imz}1}$ and Cu**BIMZ**), and the corresponding kinetics is determined. Based on the experimental results, a mechanistic cycle is derived. Then, comprehensive measurements with different monophenols are performed to investigate the monophenolase activity of the new copper complexes. The oxygenation products are identified and characterized with the help of UV/Vis and NMR spectroscopy, mass spectrometry, and fluorescence measurements. Cryogenic oxygenations of all presented model systems are performed to identify the dioxygen species involved in the catalytic cycle. Correlations between the structures of the complexes and their reactivities are discussed.

Materials and methods

Materials

All solvents were of commercially available reagent grade. Acetonitrile, dichloromethane and toluene were dried by heating to reflux under nitrogen atmosphere with calcium hydride, acetone with calcium sulfate, methanol with magnesium and tetrahydrofuran with lithium aluminium hydride. All commercial available starting materials were ordered by Sigma Aldrich Co. and ABCR. Air-sensitive compounds were prepared using standard Schlenk techniques or a MBraun LABmaster glovebox filled with nitrogen. 2-(R)-amino-3-(1*H*-imidazol-4(5)-yl)propanol dihydrochloride (histidinol dihydrochloride) was prepared according to Gynther et al. [36], 2-(1-trityl-1*H*-imidazol-4-yl)-ethyl amine was prepared according to Garibay et al. [37] and ethyl pivalimidate hydrochloride was prepared according to Allmann et al. [38]. Chromatographic purifications were performed with silica gel 60 (0.04–0.063). Flash chromatography of 4-methoxy-5-(4-methoxyphenoxy)-cyclohexa-3,5-diene-1,2-dione and 4-(*tert*-butyl)-5-(3-(*tert*-butyl)phenoxy)-cyclohexa-3,5-diene-1,2-dione was performed using an Isolera One fabricated by Biotage.

Elemental analyses

Elemental analyses were performed using a EuroEA 3000 Elemantal Analyser, fabricated by Euro Vector Instruments and Software.

Spectroscopy

UV/Vis spectra were recorded at room temperature with an Agilent 8435 Technologies photodiode array spectrophotometer. Low temperature measurements were performed in solution with an Agilent Cary 5000 spectral photometer using a CryoVAC KONTI cryostat and a quartz cell with a path length of 1 cm. NMR spectra were recorded with a Bruker Avance 400 Pulse Fourier Transform spectrometer at 300 K with a ^{1}H frequency of 400.13 MHz and a ^{13}C frequency of 100.62 MHz. Fluorescence spectra were recorded in methanol with a Perkin Elmer LS55.

Mass spectrometry

Mass spectra (ESI/MS) were recorded using a Mariner ESI-TOF mass spectrometer fabricated by Applied Biosystems. MALDI-TOF mass spectra were recorded using a Bruker Biflex III spectrometer.

Single crystal and powder x-ray diffraction

Single crystal data were recorded using a STOE Imaging Plate Diffraction System (IPDS-2) with Mo-K_α radiation ($\lambda = 0.71073$ Å) and were corrected for absorption ($T_{min/max}$: 0.8211/0.8927). The structure was solved with SHELXS-97 [39] and refined against F^2 using SHELXL-2014 [40]. All non-hydrogen atoms were refined anisotropic. The C–H and N–H H atoms were positioned with idealized geometry and refined isotropic with $U_{iso}(H) = 1.2\ U_{eq}(C,N)$ using a riding model. The absolute structure was determined and is in agreement with the selected setting [Flack x-parameter: −0.001 (18)]. One of the two crystallographically independent PF_6^- anions is disordered and was refined using a split model and restraints.

CCDC-1454612 contains the supplementary crystallographic data for this paper. These data can be obtained free charge from the Cambridge Crystallographic Data Centre via http://www.ccdc.cam.ac.uk/data_request/cif.

X-ray powder pattern were measured using a Stoe Stadi-P powder diffractometer with Cu K_α-radiation (Ge(111) monochromator) what is equipped with a MYTHEN 1 K detector.

Detection of hydrogen peroxide in catalytic catechol oxidase reactions

Hydrogen peroxide formation during the catalytic oxidation was determined by the development of the characteristic I_3^- band at 353 nm ($\varepsilon = 26{,}000$ L mol^{-1} cm^{-1}) [41] which forms upon reaction of I^- with H_2O_2. After 15 min, 1 h and 2 h, 5 mL of the reaction mixture were removed and an equal volume of water was added. The quinone was extracted three times with dichloromethane. The aqueous layer was set to pH 2 using H_2SO_4. Furthermore, 1 mL of an aqueous potassium iodide solution (10 %) and three drops of an ammonium heptamolybdate tetrahydrate solution (10 % in water) were added and UV/Vis measurements were performed directly afterwards and also every 10 min during the first 60 min of reaction time. The reaction proceeds according to the equation:

$$H_2O_2 + 2\,I^- + 2\,H^+ \rightarrow 2\,H_2O + I_2$$

$$I_{2(aq)} + I^- \rightarrow I_3^-.$$

A blank was used to account for I_3^- which is formed upon the oxidation of I^- by atmospheric oxygen.

Catalase activity measurements

Measurements of catalase activity were performed according to Monzani et al. [41]. A 0.1 M solution of hydrogen peroxide in methanol was divided in six parts. The copper(I) complexes of **L_{OL}1-3**, **L_{imz}1** and **BIMZ** (500 µM) were added and stirred for 3 h. One part was used as blank and was also stirred for 3 h. Afterwards, 5 µL of each solutions were added to 2 mL of a solution containing water (acidified to pH 2 with H_2SO_4), potassium iodide (30 mM) and ammonium heptamolybdate tetrahydrate (100 nM). After 1 h the relative intensity of the I_3^- absorption band at 353 nm as compared to the blank was measured. Catalase activity could be observed for all five complexes.

General procedure for the oxidation of 3,5-di-*tert*-butylcatechol to mimic catechol oxidase activity

Under inert atmosphere at ambient temperature, the respective copper(I) complexes were dissolved in 20 mL dichloromethane to afford a 500 µM solution. Then 10 eq. of 3,5-DTBC-H_2 were added. Subsequent injection of dioxygen into the reaction mixture started the oxidation of the catechol to the corresponding quinone, which was observed via UV/Vis and NMR spectroscopy.

General procedure for the oxygenation of external substrates to mimic tyrosinase activity

Under an inert atmosphere at ambient temperature, the respective copper(I) complexes were dissolved in 20 mL dichloromethane to afford a 500 µM solution. Then 50 eq. of the external substrate (2,4-DTBP-H, 4-MeOP-H, 3-TBP-H, NATEE, 8-hydroxyquinoline) and 100 eq. triethylamine were added. Subsequent injection of dioxygen into the reaction mixture started the conversion of the various monophenols which were monitored via UV/Vis and NMR spectroscopy.

General procedure of quenching the oxidized and oxygenated solutions

An aliquot of the reaction mixture (2.5 mL) was diluted to a 25 µM solution with dichloromethane and quenched by addition of 6 M HCl (20 mL). The phases were separated, and the aqueous phase was extracted with dichloromethane (2 × 20 mL). The combined organic fractions were dried over $MgSO_4$, filtered, and evaporated in vacuum. The residue was analyzed by NMR spectroscopy.

General procedure of kinetic measurements

Catechol oxidase activities were measured in dichloromethane saturated with dioxygen at ambient temperatures using time-dependent UV/Vis spectroscopy. In a first run solutions with concentrations of 3,5-DTBC-H_2 in a range of 1.5×10^{-3}–4×10^{-2} M were prepared. Afterwards a solution of each copper(I) complex in dichloromethane with a constant concentration of 1×10^{-3} M was added. The increasing double bands of 3,5-di-*tert*-butyl semiquinone (3,5-DTBSQ) at 377 nm and 394 nm were monitored during the first 2 min. In another series of experiments, the concentration of 3,5-DTBC-H_2 was kept constant (2.5×10^{-2} M) and the concentration of copper(I) complexes was varied in the range of 7.6×10^{-5}–1×10^{-3} M. Measurements were performed after 2 min.

Derivatization of *N*-acetyl-L-dopa ethyl ester with *ortho*-phenylenediamine

A 500 μM solution of Cu$\mathbf{L_{imz}1}$ in dichloromethane (20 mL) was treated with *N*-acetyl-L-tyrosine ethyl ester monohydrate (134.7 mg, 500.2 μmol) and triethylamine (0.14 mL 1.0 mmol). Dioxygen was bubbled through the solution continuously for 2 h. Then 10 mL of this mixture were removed and the solvent was evaporated in vacuum. Acetone (25 mL) and trifluoroacetic acid (20 mL; 1 % in water) were added and stirred for 15 min under reflux. Subsequent addition of *ortho*-phenylenediamine (13.50 mg, 123.8 μmol) afforded a yellow solution, which was stirred for 10 min under reflux. The solvent was evaporated and the residue was dissolved in methanol. Afterwards the prepared phenazine derivative was characterized by UV/Vis and fluorescence spectroscopy.

Synthesis of 4-((1*H*-imidazol-4-yl) methyl)-2-phenyl-4,5-dihydrooxyzole ($\mathbf{L_{OL}1}$)

To a solution of histidinol dihydrochloride (1.50 g, 7.00 mmol) in dry methanol (15 mL) ethyl benzimidate hydrochloride (1.13 g, 6.10 mmol, 1.3 eq.) and sodium methoxide (950 mg, 17.6 mmol, 2.5 eq.) were sequentially added and the mixture was heated at 78 °C for 2.5 h. The suspension was filtered and washed with methanol. Then, an aqueous Na_2CO_3 solution (20 mL, pH 10) was added and extracted three times with dichloromethane. The combined organic phases were dried over Na_2SO_4, and the solvent was removed by rotary evaporation. The crude product was purified by flash chromatography with chloroform/methanol (9:1, $R_f = 0.10$–0.26) as the eluent to afford $\mathbf{L_{OL}1}$ (929 mg, 4.09 mmol, 58 %) as a white powder. Anal. calcd. for $C_{13}H_{13}N_3O$: C (68.70 %); H (5.77 %); N (18.49 %); found C (68.33 %); H (6.14 %); N (18.51 %). ^{1}H-NMR (CD_3OD, 400 MHz): δ = 7.90 (dd, J = 5.3, 3.2 Hz, 2H, Ar–H), 7.60 (d, J = 1.0 Hz, 1H, imidazole H-2), 7.56–7.49 (m, 1H, Ar–H), 7.47–7.41 (m, 2H, Ar–H), 6.88 (s, 1H, imidazole H-5), 4.60 (m, 1H, –O–CH_2–C*H*–N–), 4.48 (dd, J = 9.4, 8.6 Hz, 1H, –O–CH_2–CH–N–), 4.25 (dd, J = 8.5, 7.3 Hz, 1H, –O–CH_2–CH–N–), 3.06 (dd, J = 14.6, 5.2 Hz, 1H, imidazole–CH_2–CH–), 2.81 (dd, J = 14.7, 7.9 Hz, 1H, imidazole–CH_2–CH–) ppm. ^{13}C-NMR (CD_3OD, 100 MHz): δ = 166.6 (C, 1C, –N=*C*–O–), 136.2 (CH, 1C, imidazole C-2), 134.8 (C, 1C, imidazole C-4), 133.0 (CH, 1C, phenyl C-4), 129.6 (CH, 2C, phenyl C-3, C-5), 129.3 (CH, 2C, phenyl C-2, C-6), 128.5 (C, 1C, phenyl C-1), 118.5 (CH, 1C, imidazole C-5), 73.3 (CH_2, 1C, –O–*C*H_2–CH–N–), 67.1 (CH, 1C, –O–CH_2–*C*H–N–), 33.7 (CH_2, 1C, imidazole–*C*H_2–CH–) ppm.

Synthesis of 4-((1*H*-imidazol-4-yl) methyl)-2-(*tert*-butyl)-4,5-dihydrooxyzole ($\mathbf{L_{OL}2}$)

The synthesis was performed with ethyl pivalimidate hydrochloride (1.01 g, 6.10 mmol, 1.3 eq.) as previously described. The crude product was purified by flash chromatography with dichloromethane/methanol (9:1, $R_f = 0.13$–0.29) as the eluent to afford $\mathbf{L_{OL}2}$ (667 mg, 3.22 mmol, 46 %) as a white powder. Anal. calcd. for $C_{11}H_{17}N_3O$: C (63.43 %); H (8.71 %); N (20.17 %); found C (63.15 %); H (8.84 %); N (20.41 %). ^{1}H-NMR (CD_3OD, 400 MHz): δ = 7.59 (s, 1H, imidazole H-2), 6.85 (s, 1H, imidazole H-5), 4.40–4.31 (m, 1H, –O–CH_2–C*H*–N–), 4.25 (dd, J = 9.4, 8.5 Hz, 1H, –O–CH_2–CH–N–), 4.10 (dd, J = 8.5, 6.7 Hz, 1H, –O–CH_2–CH–N–), 2.94 (ddd, J = 14.6, 4.5, 0.8 Hz, 1H, imidazole–CH_2–CH–), 2.68 (dd, J = 14.7, 7.8 Hz, 1H, imidazole–CH_2–CH–), 1.17 (s, 9H, –C(CH_3)$_3$) ppm. ^{13}C-NMR (CD_3OD, 100 MHz): δ = 177.2 (C, 1C, –N=*C*–O–), 136.1 (CH, 1C, imidazole C-2), 134.4 (C, 1C, imidazole C-4), 118.8 (CH, 1C, imidazole C-5), 73.0 (CH_2, 1C, –O–*C*H_2–CH–N–), 66.2 (CH, 1C, –O–CH_2–*C*H–N–), 34.3 (CH_2, 1C, imidazole–*C*H_2–CH–), 33.4 (C, 1C, –*C*(CH_3)$_3$), 28.1 (CH_3, 1C, –C(*C*H_3)$_3$) ppm.

Synthesis of 4-((1*H*-imidazol-4-yl) methyl)-2-methyl-4,5-dihydrooxyzole ($\mathbf{L_{OL}3}$)

The synthesis was prepared with ethyl acetimidate hydrochloride (754 mg, 6.10 mmol, 1.3 eq.) as previously described. The crude product was purified by flash chromatography with dichloromethane/methanol (9:1, $R_f = 0.31$) as the eluent to afford $\mathbf{L_{OL}3}$ (393 mg, 2.38 mmol, 34 %) as a white powder. Anal. calcd. for $C_8H_{11}N_3$: C (58.17 %); H (6.71 %); N (25.44 %); found C (57.85 %); H (6.92 %); N (25.65 %). ^{1}H-NMR (CD_3OD, 400 MHz): δ = 7.58 (s, 1H, imidazole H-2), 6.86 (s, 1H, imidazole H-5), 4.40–4.34 (m, 1H, –O–CH_2–C*H*–N–), 4.30 (dd, J = 9.4, 8.5 Hz, 1H,

–O–CH_2–CH–N–), 4.05 (dd, J = 8.3, 7.0 Hz, 1H, –O–CH_2–CH–N–), 2.94 (ddd, J = 14.7, 5.4, 0.7 Hz, 1H, imidazole–CH_2–CH–), 2.69 (dd, J = 14.7, 7.7 Hz, 1H, imidazole–CH_2–CH–), 2.69 (s, 3H, –CH_3) ppm. ^{13}C-NMR (CD_3OD, 100 MHz): δ = 168.4 (C, 1C, –N=*C*–O–), 136.1 (CH, 1C, imidazole C-2), 135.9 (C, 1C, imidazole C-4), 118.3 (CH, 1C, imidazole C-5), 73.4 (CH_2, 1C, –O–*C*H_2–CH–N–), 66.5 (CH, 1C, –O–CH_2–*C*H–N–), 33.8 (CH_2, 1C, imidazole–*C*H_2–CH–), 13.6 (CH_3, 1C, –*C*H_3) ppm.

Synthesis of *N*-(2,2-dimethylpropylidene)-2-(1-trityl-1*H*-imidazol-4-yl-)ethyl amine (L_{imz}1)

To synthesize $\mathbf{L_{imz}1}$ 2-(1-trityl-1*H*-imidazol-4-yl-) ethyl amine (1.00 g, 2.83 mmol), trimethylacetaldehyde (0.62 mL, 5.66 mmol, 2 eq.) and sodium sulfate (10.1 g, 70.7 mmol, 25 eq.) were dissolved in dry toluene (15 mL). The mixture was stirred at room temperature for at least 3 h. The residue was filtered off and washed twice with dry toluene (2 × 3 mL). The solvent was removed until a colorless solid precipitated. After 24 h the solid was filtered, washed with acetonitrile and dried in vacuum to afford $\mathbf{L_{imz}1}$ (728 mg, 1.23 mmol, 61 %) as a white powder. Anal. calcd. for $C_{29}H_{31}N_3$: C (82.62 %); H (7.41 %); N (9.97 %); found C (82.56 %); H (7.50 %); N (9.90 %). ^{1}H-NMR ($CDCl_3$, 400 MHz): δ = 7.46 (t, J = 1.2 Hz, 1H, imidazole H-2), 7.37–7.27 (m, 9H, Ar–H), 1.15–7.10 (m, 6H, Ar–H), 6.56 (s, 1H, imidazole H-5), 3.64 (t, J = 7.0 Hz, 2H, –CH_2–CH_2–N–), 2.82 (t, J = 7.0 Hz, 2H, –CH_2–CH_2–N–), 0.97 (s, 9H, –C(CH_3)$_3$) ppm. ^{13}C-NMR ($CDCl_3$, 100 MHz): δ = 172.5 (CH, 1C, –N=*C*H–C(CH_3)$_3$), 142.8 (C, 3C, phenyl C-1), 139.5 (C, 1C, imidazole C-4), 138.4 (CH, 1C, imidazole C-2), 129.9 (CH, 6C, phenyl C-3, C-5), 128.1 (CH, 6C, phenyl C-2, C-6), 128.0 (CH, 3C, phenyl C-4), 118.7 (CH, 1C, imidazole C-5), 75.2 (C, 1C, –N–*C*–(C_6H_6)$_3$), 60.6 (CH_2, 1C, –CH_2–*C*H_2–N=), 36.0 (C, 1C, =CH–*C*(CH_3)$_3$), 30.2 (CH_2, 1C, –*C*H_2–CH_2–N=), 27.1 (C, 3C, =CH–C(*C*H_3)$_3$) ppm.

Synthesis of bis(1-methylimidazol-2-yl)methane (BIMZ)

Bis(1-methylimidazol-2-yl)methane was prepared according to White et al. [35]. Anal. calcd. for $C_9H_{12}N_4$: C (61.34 %); H (6.86 %); N (31.79 %); found C (61.70 %); H (7.26 %); N (31.76 %). ^{1}H-NMR ($CDCl_3$, 400 MHz): δ = 6.89 (s, 2H, H-4), 6.76 (s, 2H, H-5), 4.21 (s, 2H, –CH_2), 3.64 (s, 6H, –CH_3) ppm. ^{13}C-NMR ($CDCl_3$, 100 MHz): δ = 143.6 (C, 2C, C-2), 127.3 (CH, 2C, C-4), 121.6 (CH, 2C, C-5), 33.2 (CH_3, 2C, *C*H_3), 27.0 (CH, 1C, *C*H_2) ppm.

Synthesis of [Cu(L_{OL}1)(CH_3CN)]PF_6

Under anaerobic conditions, $\mathbf{L_{OL}1}$ (100 mg, 0.440 mmol) was dissolved in 8 mL of acetonitrile and tetrakis-(acetonitrile)copper(I) hexafluorophosphate (164 mg, 0.440 mmol), dissolved in 5 mL acetonitrile, were added dropwise to the solution. The reaction mixture turned yellow and was stirred for 30 min under nitrogen atmosphere at ambient temperature. Subsequent evaporation to dryness yielded a yellow crystalline powder (193 mg, 0.405 mmol, 92 %). Anal. calcd. for $C_{15}H_{16}CuF_6N_4P$: C (37.78 %); H (3.38 %); N (11.75 %); found C (37.82 %); H (3.43 %); N (11.83 %). ^{1}H-NMR (CD_3CN, 400 MHz): δ = 8.20 (d, J = 7.5 Hz, 2H, Ar–H), 7.68–7.34 (m, 4H, Ar–H, imidazole H-2), 6.93 (s, 1H, imidazole H-5), 4.80 (q, J = 9.1 Hz, 1H, –O–CH_2–CH–N–), 4.40 (q, J = 10 Hz, 1H, –O–CH_2–C*H*–N–), 4.14 (dd, J = 9.7 Hz, 1H, –O–CH_2–CH–N–), 2.97 (t, J = 17.2 Hz, 1H, imidazole–CH_2–CH–), 2.74 (dd, J = 14.8, 11.5 Hz, 1H, imidazole–CH_2–CH–), 1.96 (s, 3H, –NCCH_3) ppm. ^{13}C-NMR (CD_3CN, 100 MHz): δ = 166.0 (C, 1C, –N=*C*–O–), 138.5 (C, 1C, imidazole C-4), 136.5 (CH, 1C, imidazole C-2), 133.2 (CH, 1C, phenyl C-4), 129.8 (CH, 2C, phenyl C-3, C-5), 129.3 (CH, 2C, phenyl C-2, C-6), 127.4 (C, 1C, phenyl C-1), 114.2 (CH, 1C, imidazole C-5), 73.8 (CH_2, 1C, –O–*C*H_2–CH–N–), 67.7 (CH, 1C, –O–CH_2–*C*H–N–), 33.0 (CH_2, 1C, imidazole–*C*H_2–CH–) ppm.

Synthesis of [Cu(L_{OL}2)(CH_3CN)]PF_6

[Cu($\mathbf{L_{OL}2}$)(CH_3CN)]PF_6 was prepared with $\mathbf{L_{OL}2}$ (100 mg, 0.482 mmol) and tetrakis(acetonitrile)copper(I) hexafluorophosphate (180 mg, 0.482 mmol) as described previously. The product was obtained as a white powder (192 mg, 0.420 mmol, 87 %). Anal. calcd. for $C_{11}H_{15}CuF_6N_5P$: C (34.18 %); H (4.41 %); N (12.26 %); found C (34.20 %); H (4.53 %); N (12.33 %). ^{1}H-NMR (CD_3CN, 400 MHz): δ = 7.67 (s, 1H, imidazole H-2), 6.94 (s, 1H, imidazole H-5), 4.55 (t, J = 9.2 Hz, 1H, –O–CH_2–CH–N–), 4.18–4.10 (m, 1H, –O–CH_2–C*H*–N–), 3.89 (t, J = 9.1 Hz, 1H, –O–CH_2–CH–N–), 2.86 (d, J = 15.3 Hz, 1H, imidazole–CH_2–CH–), 2.55 (dd, J = 23.1, 8.2 Hz, 1H, imidazole–CH_2–CH–), 1.96 (s, 3H, –NCCH_3), 1.34 (s, 3H, –C(CH_3)) ppm. ^{13}C-NMR (CD_3CN, 100 MHz): δ = 177.6 (C, 1C, –N=*C*–O–), 138.3 (C, 1C, imidazole C-4), 136.5 (CH, 1C, imidazole C-2), 114.6 (CH, 1C, imidazole C-5), 73.36 (CH_2, 1C, –O–*C*H_2–CH–N–), 67.1 (CH, 1C, –O–CH_2–*C*H–N–), 34.6 (C, 1C, –*C*(CH_3)$_3$), 32.9 (CH_2, 1C, –O–*C*H_2–CH–N–), 28.3 (CH_3, 1C, –C(*C*H_3)$_3$) ppm.

Synthesis of $[Cu(L_{OL}3)(CH_3CN)]PF_6$

$[Cu(\mathbf{L_{OL}3})(CH_3CN)]PF_6$ was prepared with $\mathbf{L_{OL}3}$ (100 mg, 0.605 mmol) and tetrakis(acetonitrile)copper(I) hexafluorophosphate (226 mg, 0.605 mmol) as described previously. The product was obtained as a white powder (216 mg, 0.521 mmol, 86 %). Anal. calcd. for $C_{11}H_{15}CuF_6N_5P$: C (28.96 %); H (3.40 %); N (13.51 %); found C (28.81 %); H (3.43 %); N (13.34 %). ^{1}H-NMR (CD_3CN, 400 MHz): δ = 7.67 (s, 1H, imidazole H-2), 6.95 (s, 1H, imidazole H-5), 4.59 (t, J = 8.9 Hz, 1H, –O–CH_2–CH–N–), 4.11–4.04 (m, 1H, –O–CH$_2$–CH–N–), 3.97 (t, J = 8.8 Hz, 1H, –O–CH_2–CH–N–), 2.88 (d, J = 14.9 Hz, 1H, imidazole–CH_2–CH–), 2.52 (dd, J = 14.0, 12.1 Hz, 1H, imidazole–CH_2–CH–), 2.09 (s, 3H, –CH_3), 1.96 (s, 3H, –NCCH_3) ppm. ^{13}C-NMR (CD_3CN, 100 MHz): δ = 169.2 (C, 1C, –N=C–O–), 138.5 (C, 1C, imidazole C-4), 136.9 (CH, 1C, imidazole C-2), 114.6 (CH, 1C, imidazole C-5), 72.2 (CH_2, 1C, –O–CH$_2$–CH–N–), 66.1 (CH, 1C, –O–CH$_2$–CH–N–), 33.1 (CH_2, 1C, imidazole–CH$_2$–CH–), 14.5 (C, 1C, –CH$_3$) ppm.

Synthesis of $[Cu(L_{imz}1)(CH_3CN)_2]PF_6$

$[Cu(\mathbf{L_{imz}1})(CH_3CN)_2]PF_6$ was prepared with $\mathbf{L_{imz}1}$ (100 mg, 0.237 mmol) and tetrakis(acetonitrile)copper(I) hexafluorophosphate (88.4 mg, 0.237 mmol) as described previously. The product was obtained as a white powder (159 mg, 0.223 mmol, 94 %). Anal. calcd. for $C_{11}H_{15}CuF_6N_5P$: C (55.50 %); H (5.50 %); N (9.81 %); found C (55.11 %); H (5.32 %); N (9.95 %). ^{1}H-NMR (CD_3CN, 400 MHz): δ = 7.62 (s, 1H, –N=CH–C(CH_3)), 7.51 (s, 1H, imidazole H-2), 7.42–7.35 (m, 9H, Ar–H), 7.20–7.11 (m, 6H, Ar–H), 6.79 (s, 1H, imidazole H-5), 3.64 (dd, J = 10.5, 5.2 Hz, 2H, –CH$_2$–CH_2–N–), 2.70 (dd, J = 15.1 Hz, 9.6 Hz, 2H, –CH_2–CH$_2$–N–), 1.96 (s, 6H, CH_3CN), 1.09 (s, 9H, –C(CH_3)$_3$) ppm. ^{13}C-NMR (CD_3CN, 100 MHz): δ = 177.2 (CH, 1C, –N=CH–C(CH$_3$)$_3$), 141.6 (C, 3C, phenyl C-1), 140.2 (C, 1C, imidazole C-4), 139.4 (CH, 1C, imidazole C-2), 130.5 (CH, 6C, phenyl C-3, C-5), 129.3 (CH, 3C, phenyl C-4), 129.2 (CH, 6C, phenyl C-2, C-6), 118.3 (CH, 1C, imidazole C-5), 76.9 (C, 1C, –N–C–(C$_6$H$_6$)$_3$), 62.4 (CH$_2$, 1C, –CH$_2$–CH$_2$–N=), 36.6 (C, 1C, =CH–C(CH$_3$)$_3$), 29.6 (CH$_2$, 1C, –CH$_2$–CH$_2$–N=), 27.4 (C, 3C, =CH–C(CH$_3$)$_3$) ppm.

Synthesis of $[Cu(BIMZ)(CH_3CN)]PF_6$

$[Cu(\mathbf{BIMZ})(CH_3CN)]PF_6$ was prepared with **BIMZ** (100 mg, 0.567 mmol) and tetrakis(acetonitrile)copper(I) hexafluorophosphate (212 mg, 0.567 mmol) as described previously. The product was obtained as a white powder (232 mg, 0.545 mmol, 96 %). Anal. calcd. for $C_{11}H_{15}CuF_6N_5P$: C (31.03 %); H (3.55 %); N (16.45 %); found C (31.29 %); H (3.56 %); N (16.53 %). ^{1}H-NMR (Acetone-d$_6$, 400 MHz): δ = 7.41 (s, 2H, H-4), 7.13 (s, 2H, H-5), 4.79 (s, 2H, –CH_2), 3.88 (s, 6H, –CH_3), 2.08 (s, 3H, –NCCH_3) ppm. ^{13}C-NMR (Acetone-d$_6$, 100 MHz): δ = 145.1 (C, 2C, C-2), 127.9 (CH, 2C, C-4), 124.2 (CH, 2C, C-5), 117.5 (C, 1C, –NCCH$_3$), 34.2 (CH$_3$, 2C, CH$_3$), 25.8 (CH, 1C, CH$_2$) ppm.

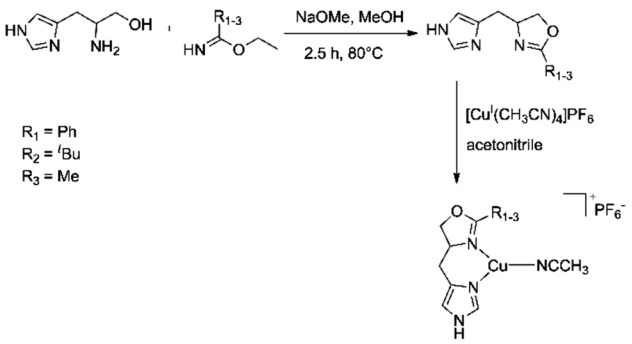

Scheme 1 Synthesis of ligands $\mathbf{L_{OL}1\text{-}3}$ and their corresponding copper(I) complexes Cu$\mathbf{L_{OL}1}$, Cu$\mathbf{L_{OL}2}$ and Cu$\mathbf{L_{OL}3}$

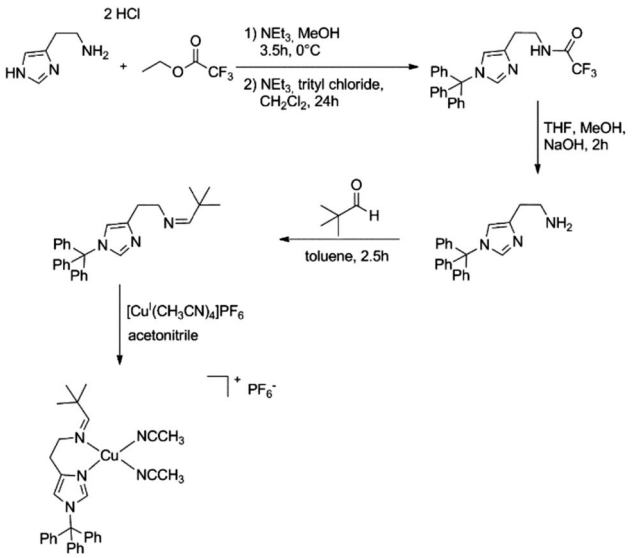

Scheme 2 Synthesis of ligand $\mathbf{L_{imz}1}$ and its corresponding copper(I) complex Cu$\mathbf{L_{imz}1}$

Synthesis of $[Cu(L_{OL}1)_2](PF_6)_2$

$[Cu(\mathbf{L_{OL}1})(CH_3CN)]PF_6$ (35.7 mg, 750 µmol) was dissolved in dry dichloromethane (25 mL). Injection of dioxygen at −78 °C for 30 min and subsequent warming to room temperature leads to a blue solution. After 3 weeks, turquoise crystals were obtained. The single crystals were of high quality and suitable for X-ray structure determination.

MS (ESI$^+$, acetone): *m/z* (%) = 517.249 [2 $\mathbf{L_{OL}1}$ + Cu]$^+$. Anal. calcd. for $C_{26}H_{26}CuF_{12}N_6O_2P_2$: C (38.65 %); H (3.24 %); N (10.40 %); found C (39.02 %); H (3.57 %); N (10.29 %).

Results

Synthesis of the ligands and their copper(I) complexes

Based on 2-(R)-amino-3-(1*H*-imidazol-4(5)-yl)-propanol dihydrochloride [36] a condensation reaction with ethyl benzimidate hydrochloride, ethyl pivalimidate hydrochloride [38] or ethyl acetimidate hydrochloride in the presence of sodium methoxide leads to the formation of three new ligands $\mathbf{L_{OL}1\text{-}3}$ (Scheme 1). Subsequent reaction with tetrakis(acetonitrile)copper(I) hexafluorophosphate generates the corresponding copper(I) complexes Cu$\mathbf{L_{OL}1\text{-}3}$.

The ligand $\mathbf{L_{imz}1}$ was prepared by an imine condensation reaction of 2-(1-trityl-1*H*-imidazol-4-yl)-ethyl amine [37] with trimethylacetaldehyde (Scheme 2). Reaction with tetrakis(acetonitrile)copper(I) hexafluorophosphate leads to the corresponding copper(I) complex Cu$\mathbf{L_{imz}1}$. In contrast to Cu$\mathbf{L_{OL}1\text{-}3}$ with one acetonitrile as co-ligand, Cu$\mathbf{L_{imz}1}$ contains two acetonitrile molecules as co-ligands.

Bis(1-methylimidazol-2-yl)methane (**BIMZ**) was synthesized as published previously [35]. Reaction with tetrakis(acetonitrile)copper(I) hexafluorophosphate leads to Cu**BIMZ** with one acetonitrile as co-ligand.

Catechol oxidase activity

The catechol oxidase activity of the new copper(I) complexes Cu$\mathbf{L_{OL}1}$, Cu$\mathbf{L_{OL}2}$, Cu$\mathbf{L_{OL}3}$, Cu$\mathbf{L_{imz}1}$, and Cu**BIMZ** was investigated first. To this end, the catalytic efficiency of all complexes towards oxidation of the substrate 3,5-di-*tert*-butylcatechol (3,5-DTBC-H_2) to 3,5-di-*tert*-butyl-*o*-benzoquinone (3,5-DTBQ) was determined. The reaction was monitored by UV/Vis spectroscopy based on the characteristic absorption band of 3,5-DTBQ at λ = 400 nm (ε = 1900 L mol^{-1} cm^{-1}) [42]. 3,5-DTBC-H_2 is well suited for catechol oxidase studies [43, 44] due to its stability, low redox potential [45–48] and the presence of bulky functional groups precluding further reactions. Consequently, it has been used in many model studies of CO as a substrate [49–55].

Catalytic runs were performed by anaerobically mixing 500 µM of the respective Cu(I) complexes in dichloromethane with 10 eq. of 3,5-DTBC-H_2 and subsequent injection of dioxygen. After the concentration of 3,5-DTBQ reached saturation, HCl quenches were performed. A small volume of each reaction mixture was removed and diluted to 25 µM with dichloromethane. 6 M hydrochloric acid was added,

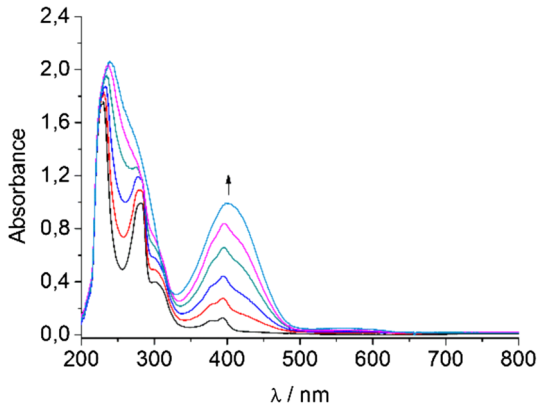

Fig. 4 UV/Vis absorption spectra obtained upon oxidation a 500 µM solution of Cu**BIMZ** in dichloromethane in the presence of 10 eq. 3,5-DTBC-H_2 during 69 h; path length (*l*) *l* = 1 mm

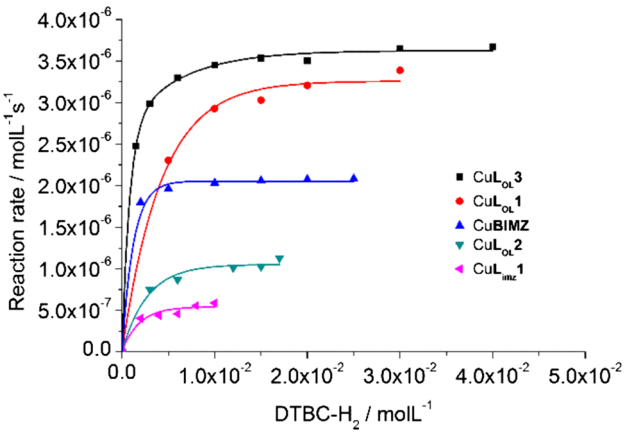

Fig. 5 Dependence of the reaction rates on the formation of 3,5-DTBSQ catalyzed by Cu$\mathbf{L_{OL}1\text{-}3}$, Cu$\mathbf{L_{imz}1}$ and Cu**BIMZ**, varying the substrate concentration. Reactions were performed in dichloromethane saturated with O_2

and the resulting solution was extracted twice with CH_2Cl_2 to eliminate all existing copper species. After removing the solvent, the resulting residue was characterized by ^{1}H-NMR and ^{13}C-NMR spectroscopy.

Monitoring the catechol oxidase activity of the five copper(I) complexes by UV/Vis spectroscopy revealed the formation of 3,5-di-*tert*-butylsemiquinone (3,5-DTBSQ) during the initial phase of the reaction, as indicated by a band with two maxima at λ = 377 and 394 nm increasing in intensity with time (Fig. 4 and Fig. S1) [48, 56].

After initial formation of 3,5-DTBSQ, subsequent oxidation to 3,5-DTBQ was observed, as evident from the formation of a band with a single maximum at λ = 400 nm. Complete conversion of 3,5-DTBC-H_2 to 3,5-DTBQ was also validated by NMR spectroscopy (Figs. S2 and S3).

Table 1 Kinetic parameters for the oxidation of 3,5-DTBC-H_2 determined from Lineweaver–Burk plots

Complex	K_M (mol L^{-1})	v_{max} (mol L^{-1} min^{-1})	k_{cat} (min^{-1})
Cu$\mathbf{L_{OL}1}$	3.01×10^{-3} ($\pm 2.50 \times 10^{-4}$)	2.23×10^{-4} ($\pm 4.53 \times 10^{-6}$)	22.3×10^{-2} ($\pm 4.53 \times 10^{-3}$)
Cu$\mathbf{L_{OL}2}$	4.19×10^{-3} ($\pm 8.60 \times 10^{-4}$)	1.11×10^{-4} ($\pm 9.65 \times 10^{-6}$)	11.1×10^{-2} ($\pm 9.65 \times 10^{-3}$)
Cu$\mathbf{L_{OL}3}$	7.43×10^{-4} ($\pm 2.12 \times 10^{-5}$)	2.22×10^{-4} ($\pm 1.07 \times 10^{-6}$)	22.2×10^{-2} ($\pm 1.08 \times 10^{-3}$)
Cu$\mathbf{L_{imz}1}$	1.04×10^{-3} ($\pm 4.47 \times 10^{-4}$)	3.56×10^{-5} ($\pm 3.35 \times 10^{-6}$)	3.56×10^{-3} ($\pm 3.36 \times 10^{-3}$)
Cu**BIMZ**	3.47×10^{-4} ($\pm 9.01 \times 10^{-6}$)	1.26×10^{-4} ($\pm 2.39 \times 10^{-7}$)	12.6×10^{-2} ($\pm 2.42 \times 10^{-4}$)

In the next step, the formation of 3,5-DTBSQ was investigated kinetically applying Michaelis–Menten theory. To this end, different concentrations of the substrate DTBC-H_2 (1.5×10^{-3}–4×10^{-2} M) were prepared in dioxygen-saturated CH_2Cl_2 and a 1×10^{-3} M solution of each Cu(I) complex was added. In agreement with typical enzyme kinetics, the resulting curves exhibit saturation characteristics (Fig. 5).

From plots of the inverse rate constant against the inverse substrate concentration (Lineweaver–Burk, Fig. S4) the kinetic parameters listed in Table 1 were obtained.

The kinetic studies allow correlations between catecholase activity and structural parameters. The three oxazoline ligands differ in their substituents, the sterical demand increasing from methyl (**$L_{OL}3$**) over phenyl (**$L_{OL}1$**) to *tert*-butyl (**$L_{OL}2$**). In agreement with these considerations, the values of v_{max} and k_{cat} reflect that Cu**$L_{OL}1$** and Cu**$L_{OL}3$** are the most active catalysts. The copper center of Cu**$L_{OL}3$** is hardly shielded by the methyl residue such that 3,5-DTBC-H_2 can bind without steric hindrance. The phenyl unit in Cu**$L_{OL}1$** is more bulky. However, due to its flexibility only a slightly higher value of K_M is observed. The much bulkier *tert*-butyl group in Cu**$L_{OL}2$**, in contrast, leads to significantly lower values for v_{max} and k_{cat}. Compared to Cu**$L_{OL}1$** and Cu**$L_{OL}3$**, Cu**$L_{imz}1$** and Cu**BIMZ** exhibited inferior catalytic activities. Moreover, the rate for Cu**BIMZ** turned out to be almost independent of the catechol concentration. This indicates a particularly high binding constant [54].

To obtain further insight into the reaction mechanism, the dependence of the formation of 3,5-DTBSQ on the complex concentration (7.6×10^{-5}–1×10^{-3} M) was studied, using an excess of substrate (2×10^{-2} M). Importantly, a linear dependence was found, implying that the reaction rate is first order in the copper complex (Fig. 6 and Fig. S5).

In addition to the characteristic double band of semiquinone, formation of an intermediate with two optical absorption bands at $\lambda = 523$ and 900 nm was observed in all kinetic measurements. These absorption features are similar to those described earlier for a purple Cu(II)-semiquinone

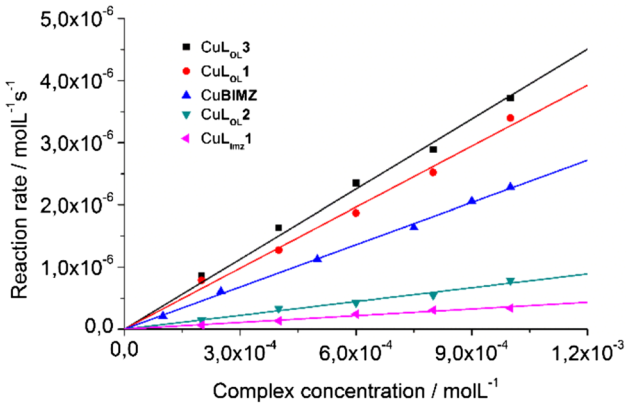

Fig. 6 Dependence of the reaction rates for the formation of 3,5-DTBSQ catalyzed by Cu**L_{OL}1-3**, Cu**$L_{imz}1$** and Cu**BIMZ** on the complex concentration. The reactions were performed in dichloromethane saturated with O_2

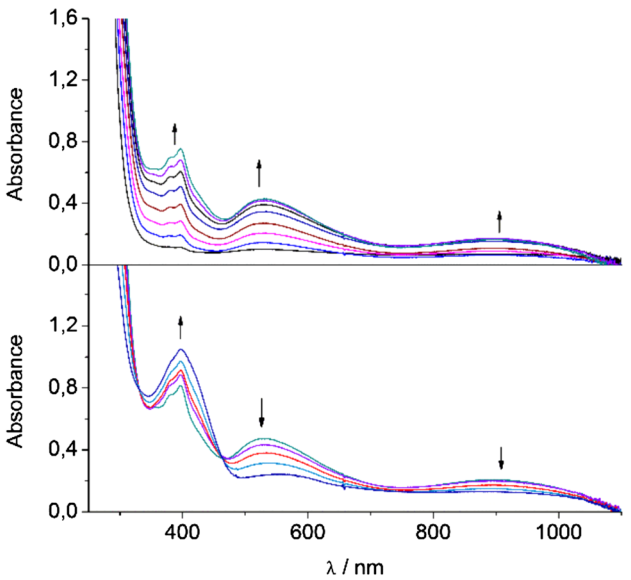

Fig. 7 UV/Vis absorption spectra obtained upon oxidation a 500 µM solution of Cu**$L_{OL}1$** and 1 eq. 3,5-DTBC-H_2 in dichloromethane saturated with O_2. *Top* optical spectra during the first 25 min; *bottom* optical spectra from 25 to 600 min; $l = 1$ mm

radical complex, which was evidenced during the catalytic oxygenation of 4-*tert*-butylphenol mediated by a Cu(DBED) complex [25]. Importantly, this complex exhibits an absorption band at λ = 545 nm and a weaker one at λ ~900 nm. Further characterization of the semiquinone complex had been achieved by mass spectrometry and single crystal structure determination.

We thus conclude that copper(II) semiquinone complexes are also formed as intermediates during the catechol oxidase reactions catalyzed by our complexes. For the Cu$\mathbf{L_{OL}1}$ system, the absorption bands of the semiquinone complex were found to be most intense. To spectroscopically monitor the buildup and the decay of [Cu(II)($\mathbf{L_{OL}1}$)(3,5-DTBSQ)]$^+$ by UV/Vis spectroscopy, the complex was generated in situ. Therefore, a 500 µM solution of Cu$\mathbf{L_{OL}1}$ was added to 1 eq. 3,5-DTBC-H_2 dissolved in dichloromethane saturated with O_2 gas (Fig. 7).

During the first 25 min an increase of the bands of the copper(II) semiquinone complex is observed. Interestingly, the formation of the semiquinone complex is accompanied by the formation of free semiquinone (Fig. 7 top and Fig. S6). After 25 min, the intensities of the bands associated with the semiquinone complex decrease, and a gradual conversion of free 3,5-DTBSQ and 3,5-DBSQ complex, respectively, to 3,5-DTBQ takes place (Fig. 7 bottom).

Visually, the buildup of the copper(II) semiquinone complex is accompanied by a color change from light yellow to purple. Subsequent decay of the semiquinone complex leads to a brown solution.

To obtain further information regarding the constitution of the Cu(II) semiquinone intermediate, an independent synthesis of [Cu(II)($\mathbf{L_{OL}1}$)(3,5-DTBSQ)]PF_6 was attempted at −60 °C. Isolation of this complex was, however, unsuccessful due to its instability at room temperature. Nevertheless, this complex could be generated in situ and detected by ESI/MS with a corresponding $m/z = 510.0$ (Fig. S7).

Combination of the experimental observations allows formulating a plausible mechanism for the catalytic pathway (Fig. 8).

Starting with the respective copper(I) complex and 3,5-DTBC-H_2, injection of dioxygen leads to the corresponding copper(II) semiquinone intermediate with the rate constant k_{cat}. The copper(II) semiquinone complex is in equilibrium with free semiquinone and a copper(II) species (equilibrium constant K_E) whence formation of the semiquinone complex and free semiquinone occur almost simultaneously (see below). Afterwards, the semiquinone converts to the product 3,5-DTBQ via the semiquinone complex with a rate constant k'.

The oxidation of the Cu(I) complex and the catechol can in principle occur under generation of H_2O or H_2O_2. Due to linear dependence of the reaction rate on the concentration

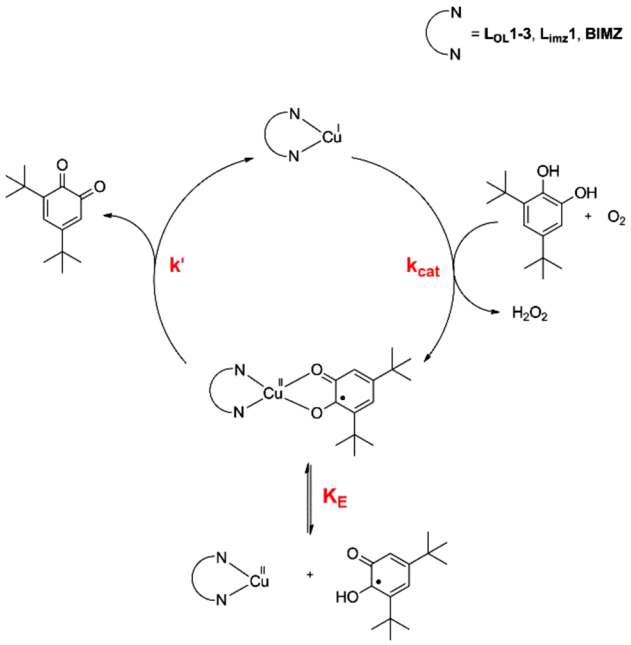

Fig. 8 Postulated mechanism for the conversion of 3,5-DTBC-H_2 to 3,5-DTBQ by different copper(I) complexes

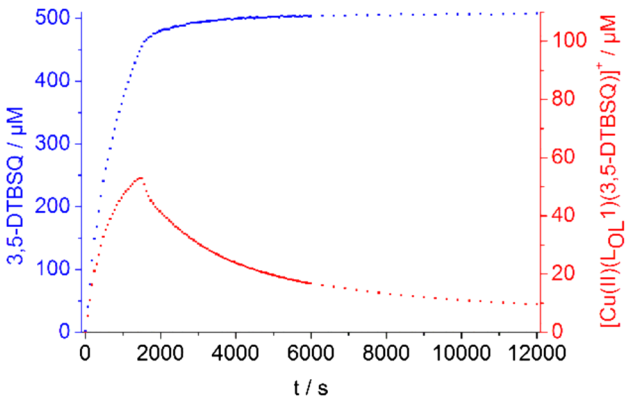

Fig. 9 *Red* Time-dependent formation and decay of [Cu(II)($\mathbf{L_{OL}1}$)(3,5-DTBSQ)]$^+$ at λ = 900 nm. *Blue* Time-dependent formation of 3,5-DTBSQ at λ = 385 nm and subsequent conversion to 3,5-DTBQ

of copper complex (see above) a mononuclear mechanism (and consequently, the formation of H_2O_2) is more likely. However, no H_2O_2 could be detected. This could be due to the fact that all copper(I) complexes exhibit catalase activity (Fig. S8).

The time-dependent formation and decay of [Cu(II)($\mathbf{L_{OL}1}$)(3,5-DTBSQ)]$^+$ are plotted along with the time-dependent buildup of 3,5-DTBSQ in Fig. 9 (see also Fig. S9). Concentration of the semiquinone complex was determined based on its absorption band at λ = 900 nm (ε = 5890 L mol^{-1} cm^{-1}), because an additional band at λ = 560 nm (related to 3,5-DTBQ) did not

allow a quantitative determination of the absorbance at $\lambda = 523$ nm ($\varepsilon = 10{,}830$ L mol^{-1} cm^{-1}). The concentration of 3,5-DTBSQ as inferred from the band at $\lambda = 385$ nm ($\varepsilon = 1900$ L mol^{-1} cm^{-1}) exhibits saturation behavior, because the subsequent conversion to 3,5-DTBQ leads to an absorption band at about the same position with a comparable intensity.

Based on the given ε-values it can be inferred that 3,5-DTBSQ and the [Cu(II)(**L$_{OL}$1**)(3,5-DTBSQ)]$^+$ complex are in equilibrium with a ratio of about 10:1. The initial slope of the buildup curve of 3,5-DTBSQ reveals a reaction rate of 3.8×10^{-5} mol L^{-1} min^{-1}. Based on the Michaelis–Menten equation a reaction rate of 3.1×10^{-5} mol L^{-1} min^{-1} is calculated for the formation of 3,5-DTBSQ mediated by Cu**L$_{OL}$1** with the parameters given in Table 1 (Fig. S10).

Furthermore, the formation of the [Cu(II)(**L$_{OL}$1**)(3,5-DTBSQ)]$^+$ complex as calculated from the initial slope (Fig. S10) results in a reaction rate of 5.3×10^{-6} mol L^{-1} min^{-1}, about one tenth of that leading to 3,5-DTBSQ. This corresponds to the ratio of maximum concentrations of free 3,5-DTBSQ and [Cu(II)(**L$_{OL}$1**)(3,5-DTBSQ)]$^+$, which are reached after 25 min reaction time (Fig. 9). The subsequent monomolecular decay of the copper(II) semiquinone complex proceeds with a first order rate constant of $k' = 1.8 \times 10^{-2}$ min^{-1} (Fig. S10), which also corresponds to formation of the final product of the catechol oxidase reaction, 3,5-DTBQ.

Tyrosinase activity

Applying well-established reaction conditions [19, 20] phenols can be catalytically oxygenated to quinones by low molecular weight model systems of tyrosinase. Following Bulkowski [57] 50 eq. of phenolic substrate and 100 eq. of triethylamine were added anaerobically to a 500 µM solution of the respective Cu(I) complex (Cu**L$_{OL}$1-3**, Cu**L$_{imz}$1,** Cu**BIMZ)** in dichloromethane, followed by injection of dioxygen at room temperature. Formation of the particular quinone was monitored by in situ UV/Vis spectroscopy based on characteristic absorption bands. After completion of the oxygenation, HCl quenches were performed and the reaction products were analyzed by NMR spectroscopy (see above).

All of the five reported copper(I) complexes were investigated regarding their ability to serve as model systems for tyrosinase. Importantly, only Cu**L$_{imz}$1** and Cu**BIMZ** were found to both stoichiometrically and catalytically convert a range of phenols to *ortho*-quinones, whereas all three oxazoline-based copper(I) complexes (Cu**L$_{OL}$1-3**) just mediate a stoichiometric conversion of 2,4-DTBP-H (Fig. S11). In the following, the two catalytically complexes and their reactivity towards five different substrates are examined in more detail.

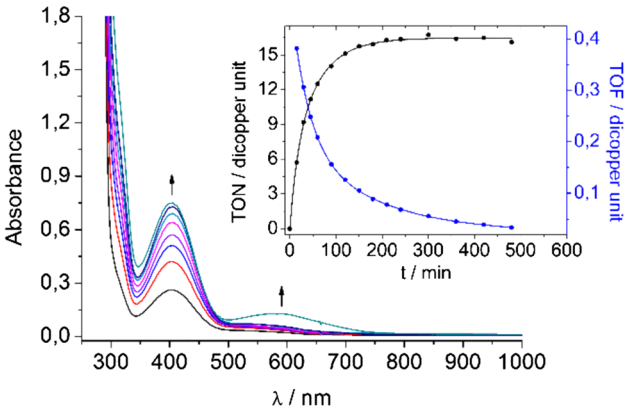

Fig. 10 UV/Vis absorption spectra obtained upon oxygenation a 500 µM solution of Cu**L$_{imz}$1** in dichloromethane in the presence of 50 eq. 2,4-DTBP-H and 100 eq. triethylamine; $l = 1$ mm. *Insert* TON and TOF

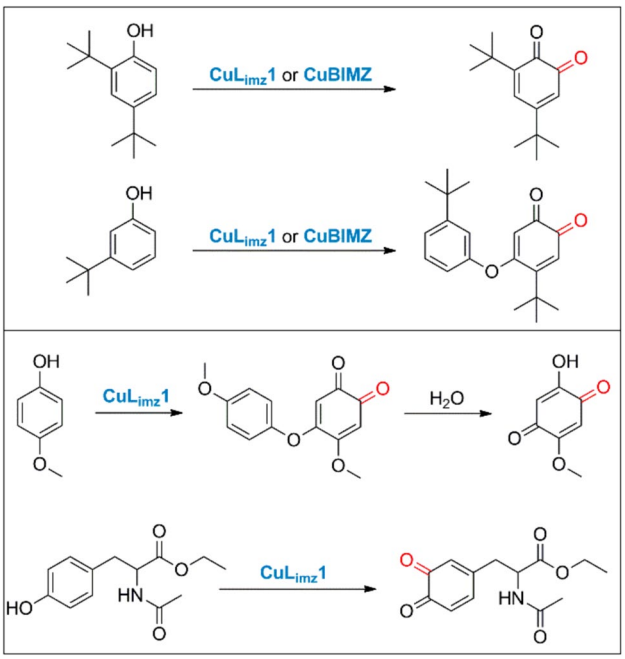

Scheme 3 Schematic illustration of different substrates oxygenated by Cu**L$_{imz}$1** and Cu**BIMZ**

The first employed substrate, 2,4-di-*tert*-butylphenol (2,4-DTBP-H), is sterically encumbered but widely used due to the stability of the resulting quinone. Oxygenation of Cu**L$_{imz}$1** leads to the formation of 3,5-DTBQ with an absorption band at $\lambda = 403$ nm ($\varepsilon = 1830$ L mol^{-1} cm^{-1}) [19] (Fig. 10; Scheme 3).

Oxygenation was complete after about 3 h, resulting in a turnover number of 16. Conversion of the same substrate by Cu**BIMZ** leads to the appearance of an absorption band with two maxima at $\lambda = 378$ and 396 nm during

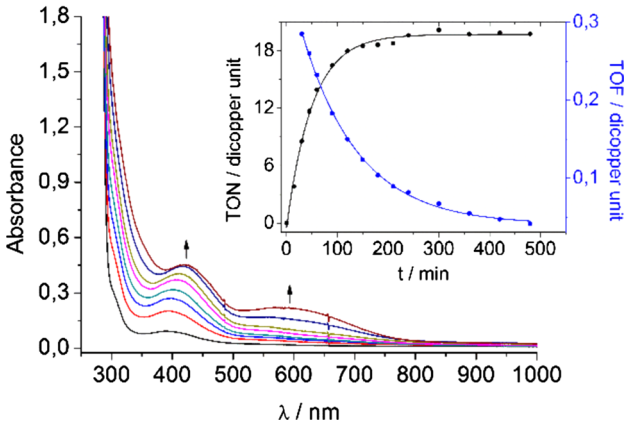

Fig. 11 UV/Vis absorption spectra obtained upon oxygenation a 500 μM solution of Cu$\mathbf{L_{imz}1}$ in dichloromethane in the presence of 50 eq. 3-TBP-H and 100 eq. triethylamine; $l = 1$ mm. *Insert* TON and TOF

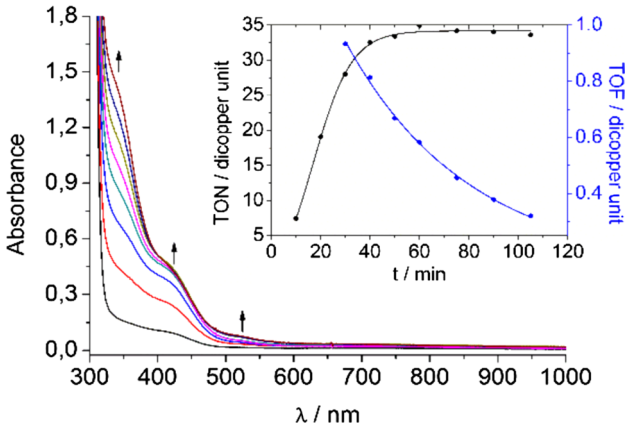

Fig. 12 UV/Vis absorption spectra obtained upon oxygenation a 500 μM solution of Cu$\mathbf{L_{imz}1}$ in dichloromethane in the presence of 50 eq. 4-MeOP-H and 100 eq. triethylamine; $l = 1$ mm. *Insert* TON and TOF

the first 2 h, indicating formation of free 3,5-DTBSQ (Fig. S12) [47, 48, 56]. This feature changes to a single band at $\lambda = 403$ nm, indicating conversion to 3,5-DTBQ the formation of which is completed after 6 h with a TON of 9. The resulting NMR spectra (Fig. S13 and S14 for Cu$\mathbf{L_{imz}1}$; Fig. S15 and S16 for Cu**BIMZ**) confirm the formation of 3,5-DTBQ as well as the C–C coupling product 3,3′,5,5′-tetra-*tert*-butyl-2,2′-biphenol and unreacted 2,4-DTBP-H in a ratio of 13:35:52 for Cu$\mathbf{L_{imz}1}$ and 5:42:53 for Cu**BIMZ**.

For both the Cu$\mathbf{L_{imz}1}$ and the Cu**BIMZ** system, a broad band at $\lambda = 600$ nm emerges at the end of the catalytic runs. To check whether this absorption band derives from a copper triethylamine complex that limits the turnover number, because it is unreactive towards substrate, an exchange of triethylamine against 1,8-diazabicyclo[5.4.0]undec-7-ene (DBU) and subsequent oxygenation of 2,4-DTBP-H by Cu$\mathbf{L_{imz}1}$ was accomplished. The UV/Vis spectra show no absorption band at 600 nm after completion of the reaction (Fig. S17) but the same turnover number is achieved (TON = 16). This leads to the conclusion that triethylamine is involved in the formation of the absorption band, but only after the conversion of 2,4-DTBP-H to 3,5-DTBQ is completed. Consequently, the formation of the unreactive end product does not limit the activity of the catalytic system.

The next investigated substrate was 3-*tert*-butylphenol (3-TBP-H). Oxygenation of 3-TBP-H with Cu$\mathbf{L_{imz}1}$ and Cu**BIMZ** first leads to a band at $\lambda = 400$ nm the maximum of which subsequently shifts to $\lambda = 425$ nm where it stays until saturation (Fig. 11 for Cu$\mathbf{L_{imz}1}$; Fig. S18 for Cu**BIMZ**).

This observation suggests the initial formation of 4-*tert*-butylquinone [58] and further reaction to the coupled *ortho*-quinone 4-(*tert*-butyl)-5-(3-(*tert*-butyl)phenoxy) cyclohexa-3,5-diene-1,2-dione [21, 22] with a TON of 20 for Cu$\mathbf{L_{imz}1}$ and a TON of 6 for Cu**BIMZ** ($\varepsilon = 898$ L mol^{-1} cm^{-1} at $\lambda = 425$ nm). The corresponding NMR spectra (Figs. S19 and S20 for Cu$\mathbf{L_{imz}1}$; Figs. S21 and S22 for Cu**BIMZ**) validate the presence of the coupled *ortho*-quinone besides unreacted 3-TBP-H (Scheme 3). Importantly, no C–C coupling product was detected. The formation of a broad band at $\lambda = 600$ nm was also observed for this system after completion of the oxygenation reaction.

To study the electronic influence of substituents in the applied substrate, catalytic runs were performed using 4-methoxyphenol (4-MeOP-H). Based on the pronounced mesomeric (+M) effect [59], very rapid conversion of 4-MeOP-H to the coupled quinone 4-methoxy-5-(4-methoxyphenoxy)cyclohexa-3,5-diene-1,2-dione was observed (Fig. 12).

In the case of Cu$\mathbf{L_{imz}1}$, oxygenation with subsequent reaction to the coupled product proceeds with a TON of 34 ($\varepsilon = 524$ L mol^{-1} cm^{-1}, $\lambda = 418$ nm) after 60 min. NMR spectra (Figs. S23, S24) confirm the existence of the coupled quinone besides the educt. The course of the reaction was also followed for additional 3 h. Hydrolysis through water formed during the catalytic run yielded the *para*-quinone 2-hydroxy-5-methoxy-[1, 4] benzoquinone which was also detected by NMR spectroscopy (Fig. S25 and S26) [60].

Oxygenation of 4-MeOP-H with Cu**BIMZ** also leads to rapid emergence of an absorption band at $\lambda = 418$ nm which saturates after 40 min (Fig. S27). Further oxygenation generates an additional absorption band at approximately $\lambda = 465$ nm, rising in intensity for 6 days. A first NMR spectrum taken after 40 min indicates that the coupled quinone 4-methoxy-5-(4-methoxyphenoxy) cyclohexa-3,5-diene-1,2-dione is formed, accompanied by

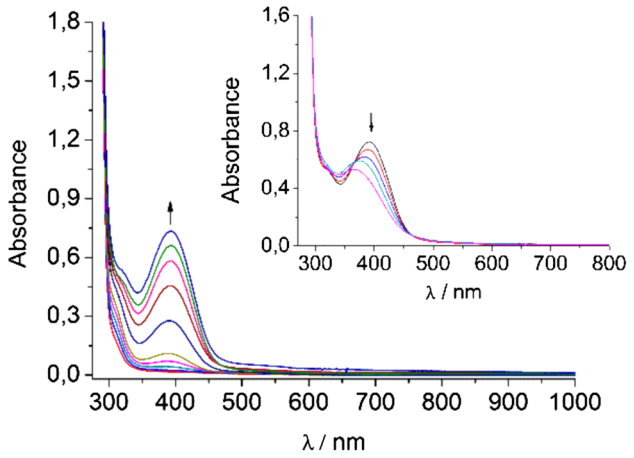

Fig. 13 UV/Vis absorption spectra obtained upon oxygenation a 500 µM solution of Cu$\mathbf{L_{imz}1}$ in dichloromethane in the presence of 50 eq. NATEE and 100 eq. triethylamine; $l = 1$ mm. *Insert* decrease of the absorption band after 4 h

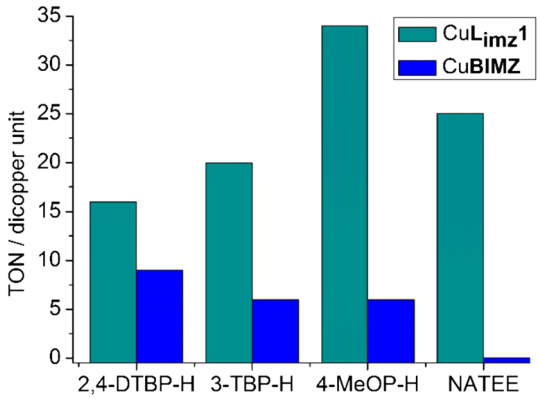

Fig. 14 Quantification of the conversion of different monophenols to the corresponding *ortho*-quinones

2-hydroxy-5-methoxy-[1, 4] benzoquinone and further by-products (Figs. S28, S29). A turnover number of six was calculated at this reaction time; due to the mixture of products, however, this result is problematic. After 5 h another HCl quench shows a variety of undefined products (Figs. S30 and S31). Based on these observations, Cu**BIMZ** cannot be considered as a selective catalyst for the oxygenation of 4-MeOP-H.

The substrate *N*-acetyl-L-tyrosine ethyl ester monohydrate (NATEE) provides an analog to the native substrate tyrosine, and therefore, is of significant interest regarding model systems of tyrosinase. The conversion to the corresponding dopaquinone mediated by Cu$\mathbf{L_{imz}1}$ proceeds with a maximal TON of 25 ($\varepsilon = 1188$ L mol^{-1} cm^{-1}, $\lambda = 392$ nm) [61] (Fig. 13). The rise the *ortho*-quinone absorption band at $\lambda = 392$ nm exhibits a sigmoidal fashion (Fig. S32). After 4 h, the intensity of the absorption band decreases again and its maximum shifts to $\lambda = 358$ nm, indicating conversion of the *N*-acetyl-L-dopa ethyl ester into a product the identity of which could not be established by NMR spectroscopy [27].

For further identification of the primary oxygenation product *N*-acetyl-L-dopa ethyl ester dichloromethane was removed from the reaction mixture after 2 h and the residue analyzed with mass spectrometry. The peak at $m/z = 268.2$ [M + H] can be assigned to the corresponding catechol (Fig. S33). However, this result did not give any information regarding the regioselectivity of the hydroxylation. Derivatization to the corresponding phenazine using *ortho*-phenylenediamine permits the identification of *ortho*-quinones via fluorescence spectroscopy. Based on a fluorescence band at $\lambda = 523$ nm and an absorption band at $\lambda = 380$ nm in the UV/Vis (Fig. S34), which are in the range of known phenazine derivatives, *ortho*-hydroxylation could be confirmed unequivocally [62, 63]. Surprisingly, Cu**BIMZ** exhibited no tyrosinase activity in the case of NATEE.

Figure 14 gives an overview of the conversion of the investigated monophenols to *ortho*-quinones. Importantly, Cu$\mathbf{L_{imz}1}$ globally exhibits a much higher catalytic activity than Cu**BIMZ**. Moreover, as exemplified for the substrate 4-MeOP-H, it is much more selective. These findings are attributed to the higher flexibility of the ligand backbone of $\mathbf{L_{imz}1}$ as compared to **BIMZ** which facilitates formation of the ternary intermediate required for hydroxylation of the substrate (see above) [2, 17–19, 64].

To expand the scope of potential substrates, 8-hydroxyquinoline was also examined [65]. Following the standard oxygenation protocol, both Cu$\mathbf{L_{imz}1}$ and Cu**BIMZ** instantaneously produced an absorption band at $\lambda = 412$ nm which did not change in time any more (Fig. S35). NMR spectra taken after the HCl quenches revealed no indication for the formation of *ortho*-quinone as product. To obtain more information on this issue, the reaction product was isolated by flash chromatography with dichloromethane ($R_f = 0.31$). The corresponding NMR spectra also exclude the formation of quinone (Figs. S36 and S37). Due to the high tendency of 8-hydroxyquinoline to form stable metal complexes we conclude that no hydroxylation occurred. Instead, the ligands $\mathbf{L_{imz}1}$ and **BIMZ** are replaced by 8-hydroxyquinoline to form the homoleptic square planar complex [Cu(II)(8-quinolinol)$_2$]. The identity of the product was clarified via mass spectrometry $m/z = 415.09$ and powder diffractometry; the measured pattern is in full agreement with the calculated diffraction pattern based on the published structure (Fig. S38) [66].

μ-Peroxo and other Cu(II) species

The μ-η^2:η^2-peroxo-dicopper(II) complex is the most important reactive intermediate in the mechanistic cycle of tyrosinase [1, 2]. For a new ligand system, it is necessary to determine the active copper peroxide species. In the case of tyrosinase, the copper(I) ions are oxidized to copper(II) ions and bind dioxygen as peroxide in a characteristic side-on geometry (μ-η^2:η^2) [12, 22, 65]. The intense absorption band between λ = 340–380 nm is due to an in-plane $\pi_\sigma^* \rightarrow d_{x^2-y^2}$ charge transfer transition, and the less intense absorption feature between λ = 510–580 nm to an out-of-plane $\pi_v^* \rightarrow d_{x^2-y^2}$ peroxo to copper(II) charge transfer transition [1, 2, 20].

To obtain spectroscopic information regarding these intermediates, 3 mM solutions of each copper(I) complex (Cu$\mathbf{L_{OL}}$**1-3**, Cu$\mathbf{L_{imz}}$**1** and Cu**BIMZ**) in acetone and dichloromethane were cooled to −85 °C under nitrogen atmosphere. After injection of O_2 gas intense optical absorption bands between λ = 333 and 357 nm were observed in the UV/Vis spectra (Fig. S39). The position of the maxima differs only slightly. Specifically, the μ-η^2:η^2-peroxo-dicopper(II) complex of Cu$\mathbf{L_{OL}}$**1** and Cu$\mathbf{L_{OL}}$**3** exhibit LMCT bands at λ = 357 nm and λ = 335 nm in acetone which can be associated with in-plane $\pi_\sigma^* \rightarrow d_{x^2-y^2}$ charge transfer transitions. Additional absorption bands at λ = 600 nm in the case of Cu$\mathbf{L_{OL}}$**1** and λ = 510 nm in the case of Cu$\mathbf{L_{OL}}$**3** are due to out-of-plane $\pi_v^* \rightarrow d_{x^2-y^2}$ peroxo to copper(II) charge transfer transitions. Cu$\mathbf{L_{OL}}$**2** and Cu**BIMZ** were measured in dichloromethane and exhibited absorption maxima at λ = 340 nm and λ = 610 nm for Cu$\mathbf{L_{OL}}$**2** and λ = 333 nm as well as λ = 600 nm for Cu**BIMZ**. The slight shift of the $\pi_\sigma^* \rightarrow d_{x^2-y^2}$ charge transfer transition to higher energies was also noticed for copper(I) complexes with bidentate bis(oxazoline) ligands [67]. In contrast, no μ-η^2:η^2-peroxo-dicopper(II) complex could be found for Cu$\mathbf{L_{imz}}$**1** in tetrahydrofuran, dichloromethane, and acetone.

In previous publications, we correlated a high stability of the peroxo intermediates with a low catalytic reactivity and vice versa. Specifically, for model systems with a high catalytic activity the peroxo intermediate turned out to be hardly detectible [30]. This also appears to be correct for the present study as Cu$\mathbf{L_{imz}}$**1** is the most active tyrosinase catalyst described in this paper.

In an attempt to generate the peroxide core for Cu$\mathbf{L_{OL}}$**1** in dichloromethane no characteristic absorption band was obtained after injection of O_2. Instead, blue single crystals, suitable for single crystal structure determination were obtained from the solution within 3 weeks. The resulting complex [Cu($\mathbf{L_{OL}}$**1**)$_2$](PF$_6$)$_2$ crystallizes in the orthorhombic space group $P2_12_12_1$ with four formula units per unit cell and all atoms in general positions (Fig. 15).

Selected crystallographic parameters and details of the structure refinement as well as lists with selected bond lengths and angles are presented in Tables S1–S4. In the crystal structure, the copper(II) cations are fourfold coordinated by each two N-atoms of two $\mathbf{L_{OL}}$**1** ligands, within a strongly distorted square planar geometry. The Cu–N bond lengths are between 1.958 (4) and 1.996 (4) Å and are in the typical range for known bidentate homoleptic copper(II) complexes [68]. The angles range from 91.12 (18)° to 159.4 (2)°.

Summary and conclusion

Five new small molecule model systems (Cu$\mathbf{L_{OL}}$**1-3,** Cu$\mathbf{L_{imz}}$**1** and Cu**BIMZ**) have been synthesized and investigated regarding their catechol oxidase and tyrosinase activities. The results are summarized graphically in Fig. 16. Based on the mechanistic cycle in Fig. 8, all of these copper(I) complexes oxidize 3,5-DTBC-H_2 to the corresponding quinone (Fig. 16). A copper(II) semiquinone species and free 3,5-DTBSQ have been identified as intermediates during these reactions. Kinetic measurements for the formation of semiquinone applying Michaelis–Menten approach revealed a sequence of activity in the order Cu$\mathbf{L_{OL}}$**3** ≈ Cu$\mathbf{L_{OL}}$**1** > Cu**BIMZ** > Cu$\mathbf{L_{OL}}$**2** > Cu$\mathbf{L_{imz}}$**1**.

Whereas Cu$\mathbf{L_{imz}}$**1** and Cu**BIMZ** also exhibit catalytic tyrosinase activity, the copper(I) complexes supported by the ligands $\mathbf{L_{OL}}$**1-3** only mediate stoichiometric conversions of 2,4-DTBP-H to the corresponding *ortho*-quinone. This indicates that release of the product is hindered in the stoichiometric systems, in contrast to the catalytic tyrosinase model. Importantly, μ-η^2:η^2-peroxo intermediates of Cu$\mathbf{L_{OL}}$**1-3** and Cu**BIMZ** could be detected, whereas this was not possible for the most active tyrosinase catalyst, Cu$\mathbf{L_{imz}}$**1**. These findings provide evidence for the hypothesis that the reaction pathway proceeds via side-on peroxo intermediates [12, 19, 69].

To further explore the catalytic activity of the first two systems several monophenols were employed as substrates. For the oxygenation of 2,4-DTBP-H to 3,5-DTBQ a TON of 16 was derived for Cu$\mathbf{L_{imz}}$**1** and 9 for Cu**BIMZ**. In contrast to mere oxygenation, the conversion of less substituted monophenols, such as 3-TBP-H and 4-MeOP-H led to *ortho*-hydroxylation with subsequent two-electron oxidation, followed by a coupling reaction in 5-position.

From a biomimetic perspective, the reactivity with regard to the substrate NATEE was of particular interest. Surprisingly, only Cu$\mathbf{L_{imz}}$**1** showed tyrosinase activity with respect to this substrate, exhibiting a turnover number of 25 after 4 h. The combination of an imidazole and an imine unit thus appears to be more efficient as compared to the

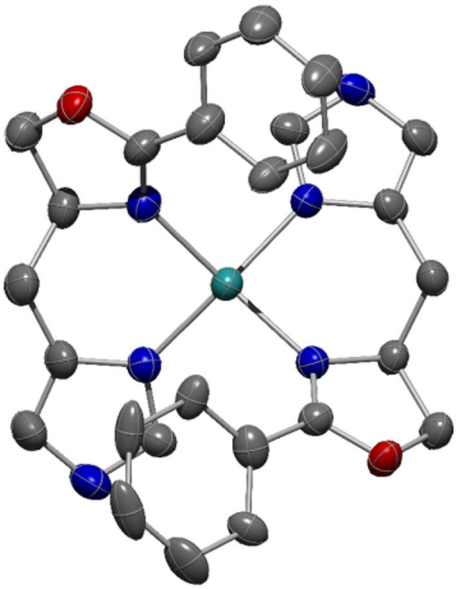

Fig. 15 Crystal structure of $[Cu(II)(\mathbf{L_{OL}1})_2](PF_6)_2$; H atoms are omitted for clarity. *Color code*: *C* gray; *N* blue; *O* red; *Cu* turquoise

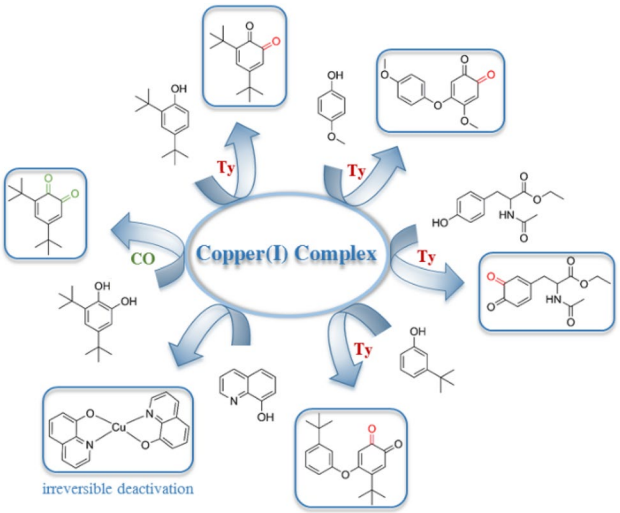

Fig. 16 Overview of the conversion of a variety of substrates and their corresponding products using the reported new copper(I) complexes

combination of two imidazole rings bridged by a methyl group. We again attribute the difference in tyrosinase activity to the higher flexibility of the Cu$\mathbf{L_{imz}1}$ system, which is necessary for the hydroxylation step. By contrast, the increased rigidity of Cu**BIMZ** leads to a significantly lower reactivity, independent of the used monophenol. For the substrate 4-MeOP-H, the decreased reactivity of Cu**BIMZ** resulted in a variety of products during the catalytic mechanism; i.e., a loss of specificity.

An irreversible deactivation was observed during the reaction of both copper(I) complexes with 8-hydroxyquinoline. The high tendency of 8-hydroxyquinoline to generate stable metal complexes led to a displacement of the respective ligands, resulting in the homoleptic [Cu(II)(8-quinolinol)$_2$] complex. From the homoleptic complex $[Cu(\mathbf{L_{OL}1})_2](PF_6)_2$, we presented a new crystal structure.

In summary, the results of our study demonstrate the importance of structural factors (flexibility of the ligand backbone and presence of bulky substituents) on the catalytic activity of model systems of tyrosinase. The catechol oxidase reaction is less sensitive with respect to these steric effects. Moreover, the activities of the model systems of tyrosinase are found to critically depend on the ability of the catalyst to release the oxygenated product as quinone. Further, fine-tuning of the catalytic activity can be achieved by variation of the electronic structure of the ligand, in particular, the donor/acceptor properties of the employed heterocyclic units.

Acknowledgments We express our gratitude to Deutsche Forschungsgemeinschaft (DFG), CAU Kiel and COST CM 1003 for support of this research. Thanks to Miriam Schehr for the introduction to operate with the Isolera One fabricated by Biotage, Marcel Dommaschk for the help measuring the fluorescence spectra and Michael Wendt for performing the XRPD measurements.

Compliance with ethical standards

Conflict of interest Authors declare that there are no conflicts of interests.

References

1. Solomon EI, Sundaram UM, Machonkin TE (1996) Chem Rev 96:2563–2605
2. Rolff M, Schottenheim J, Decker H, Tuczek F (2011) Chem Soc Rev 40:4077–4098
3. Decker H, Schweikardt T, Tuczek F (2006) Angew Chem Int Ed 45:4546–4550
4. Sánchez-Ferrer Á, Rodríguez-López JN, García-Cánovas F, García-Carmona F (1995) Biochim Biophys Acta 1247:1–11
5. Wu B (2014) Curr Top Med Chem 14:1425–1449
6. Simon JD, Peles D, Wakamatsu K, Ito S (2009) Pigment Cell Melanoma Res 22:563–579
7. Loizzo MR, Tundis R, Menichini F (2012) Compr Rev Food Sci Food Saf 11:378–398
8. van Holde KE, Miller KI, Decker H (2001) J Biol Chem 276:15563–15566
9. Solem E, Tuczek F, Decker H (2016) Angew Chem 128:2934–2938
10. Réglier M, Jorand C, Wagell B (1990) J Chem Soc Chem Commun 24:1752–1755
11. Casella L, Gullotti M, Bartosek M, Pallanza G, Laurenti E (1991) J Chem Soc Chem Commun 18:1235–1237
12. Battaini G, De Carolis M, Monzani E, Tuczek F, Casella L (2003) J Chem Soc Chem Commun 6:726–727
13. Battaini G, Monzani E, Casella L, Lonardi E, Tepper AWJW, Canters GW, Bubacco L (2002) J Biol Chem 277:44606–44612

14. Palavicini P, Granata A, Monzani E, Casella L (2005) J Am Chem Soc 127:18031–18036
15. Spada A, Palavicini S, Monzani E, Bubacco L, Casella L (2009) Dalton Trans 2009:6468–6471
16. Garcia-Bosch I, Company A, Frisch JR, Torrent-Sucarrat M, Cardellach M, Gamba I, Gìell M, Casella L, Que L Jr, Ribas X, Luis JM, Costas M (2010) Angew Chem Int Ed 49:2406–2409
17. Mirica LM, Vance M, Rudd DJ, Hedman B, Hodgson KO, Solomon EI, Stack TDP (2005) Science 308:1890–1892
18. Op't Holt BT, Vance MA, Mirica LM, Heppner DE, Stack TDP, Solomon EI (2009) J Am Chem Soc 131:6421–6438
19. Rolff M, Schottenheim J, Peters G, Tuczek F (2010) Angew Chem Int Ed 49:6438–6442
20. Hoffmann A, Citek C, Binder S. Goos A, Rübhausen M, Troeppner O, Ivanovic-Burmazovic I, Wasinger EC, Stack TDP, Herres-Pawlis S (2013) Angew Chem Int Ed 52:5398–5401
21. Esguerra KVN, Fall Y, Lumb JP (2014) Angew Chem Int Ed 53:5877–5881
22. Askari MS, Rodriguez-Solano LA, Proppe A, McAllister B, Lumb JP, Otterwaelder X (2015) Dalton Trans 44:12094–12097
23. Xu B, Lumb JP, Arndtsen BA (2015) Angew Chem Int Ed 54:4208–4211
24. Esguerra KVN, Fall Y, Petijean L, Lumb JP (2014) J Am Chem Soc 136:7662–7668
25. Askari MS, Esguerra KVN, Lumb JP, Ottenwaelder X (2015) Inorg Chem 54:8665–8672
26. Huang Z, Kwon O, Esguerra KVN, Lumb JP (2015) Tetrahedron 71:5871–5885
27. Hamann JN, Schneider R, Tuczek F (2015) J Coord Chem 68:3259–3271
28. Schottenheim J, Gernert C, Herzigkeit B, Krahmer J, Tuczek F (2015) Eur J Inorg Chem 2015:3501–3511
29. Hamann JN, Rolff M, Tuczek F (2015) Dalton Trans 44:3251–3258
30. Hamann JN, Tuczek F (2014) Chem Commun 50:2298–2300
31. Schottenheim J, Fateeva N, Thimm W, Krahmer J, Tuczek F (2013) Z Allg Anorg Chem 8:1491–1497
32. Rolff M, Hamann JN, Tuczek F (2011) Angew Chem 123:7057–7061
33. Rolff M, Schottenheim J, Tuczek F (2010) J Coord Chem 63:2382–2399
34. Rolff M, Tuczek F (2008) Angew Chem 120:2378–2381
35. Braussaud N, Rüther T, Cavell KJ, Skelton BW, White AH (2001) Synthesis 4:626–632
36. Kovalainen JT, Christiaans JAM, Kotisaari S, Laitinen JT, Männistö PT, Tuomisto L, Gynther J (1999) J Med Chem 42:1193–1202
37. Garibay PW (2011) US 2011/0166321 A1
38. Kupfer R, Nagel M, Wuerthwein EU, Allmann R (1985) Chem Ber 118:3089–3104
39. Sheldrick GM (2008) Acta Crystallogr Sect A Found Crystallogr 64:112–122
40. Sheldrick GM (2015) Acta Crystallogr C 71:3–8
41. Monzani E, Quinti L, Perotti A, Casella L, Gullotti M, Randaccio L, Geremia S, Nardin G, Faleschini P, Tabbi G (1998) Inorg Chem 37:553–562
42. Mukherjee J, Mukherjee R (2002) Inorg Chim Acta 337:429–438
43. Nevesa A, Rossi LM, Bortoluzzi AJ, Szpoganicz B, Wiezbicki C, Schwingel E (2002) Inorg Chem 41:1788–1794
44. Sénèque O, Campion M, Douziech B, Giorgi M, Rivière E, Journaux Y, Le Mest Y, Reinaud O (2002) Eur J Inorg Chem 8:2007–2014
45. Rall J, Wanner M, Albrecht M, Hornung FM, Kaim W (1999) Chem Eur J 5:2802–2809
46. Horner L, Geyer E (1965) Chem Ber 98:2016–2045
47. Harmalker S, Jones SE, Sawyer DT (1983) Inorg Chem 22:2790–2794
48. Stallings MD, Morrison MM, Sawyer DT (1981) Inorg Chem 20:2655–2660
49. Gentschev P, Müller N, Krebs B (2000) Inorg Chim Acta 300:422–452
50. Zippel F, Ahlers F, Werner R, Haase W, Nolting HF, Krebs B (1996) Inorg Chem 35:3409–3419
51. Wegner R, Gottschaldt M, Görls H, Jäger EG, Klemm D (2000) Angew Chem 112:608–612
52. Kao CH, Wie HH, Liu YH, Lee GH, Wang Y, Lee CJ (2001) J Inorg Biochem 84:171–178
53. Wegner R, Gottschaldt M, Görls H, Jäger EG, Klemm D (2001) Chem Eur J 7:2143–2157
54. Ackermann J, Meyer F, Kaifer E, Pritzkow H (2002) Chem Eur J 8:247–258
55. Manzur J, Garcia AM, Rivas V, Atria AM, Valenzuela J, Spodine E (1997) Polyhedron 16:2299–2301
56. Jovanovic SV, Kónya K, Scaiano JC (1995) Can J Chem 73:1803–1810
57. Bulkowski JE (1985) US patent 4545937
58. Ramadan AEMM, Youssef S, Eissa H (2014) Int J Adv Res 2:116–130
59. Clayden J, Greeves N, Warren S (2012) Organic chemistry. Oxford University Press, Oxford
60. Nilges MJ, Swartz HM, Riley PA (1984) J Biol Chem 259:2446–2451
61. Taylor SW, Molinski TF, Rzepecki LM, Waite JH (1991) J Nat Prod 54:918–922
62. Badger GM, Walker IS (1956) J Chem Soc, pp 122–126
63. Zhu JH, Olmstead JA, Gray DG (1995) J Wood Chem Technol 15:43–64
64. Matoba Y, Kumagai T, Yamamoto A, Yoshitsu H, Sugiyama M (2006) J Biol Chem 281:8981–8990
65. Wilfer C, Liebhäuser P, Hoffmann A, Erdmann H, Grossmann O, Runtsch L, Paffenholz E, Schepper R, Dick R, Bauer M, Dürr M, Ivanovic-Burmazovic I, Herres-Pawlis S (2015) Chem Eur J 21:17639–17649
66. Palenik GJ (1964) Acta Cryst 17:687–695
67. Walli A, Dechert S, Bauer M, Demeshko S, Meyer F (2014) Eur J Inorg Chem 2014:4660–4676
68. Li J, Widlicka DW, Fichter K, Reed DP, Weisman GR, Wong EH, DiPasquale A, Heroux KJ, Golen JA, Reinhold AL (2010) Inorg Chim Acta 364:185–194
69. Santagostini L, Gullotti M, Monzani E, Casella L, Dillinger R, Tuczek F (2000) Chem Eur J 6:519–522